THE JOURNAL OF PHYSICAL CHEMISTRY A

Article

pubs.acs.org/JPCA

Multireference Ab Initio Study of the Ground and Low-Lying Excited States of $Cr(CO)_2$ and $Cr(CO)_3$

Joonghan Kim,*[,†] Jeongho Kim,[‡] and Hyotcherl Ihee*[,§,∥]

[†]Department of Chemistry, The Catholic University of Korea, Bucheon, 420-743, Republic of Korea

[‡]Department of Chemistry, Inha University, Incheon, 402-751, Republic of Korea

[§]Center for Nanomaterials and Chemical Reactions, Institute for Basic Science, Daejeon, 305-701, Republic of Korea

[∥]Department of Chemistry, KAIST, Daejeon, 305-701, Republic of Korea

Supporting Information

ABSTRACT: We investigate the ground and low-lying excited states of unsaturated chromium carbonyls, $Cr(CO)_2$ and $Cr(CO)_3$, using multiconfigurational ab initio perturbation theory. Unlike other chromium carbonyls, there are discrepancies between the experiment and theory on the identity of the ground states of $Cr(CO)_2$ and $Cr(CO)_3$. From multireference ab initio calculations considering the full valence orbitals of $Cr(CO)_2$ and $Cr(CO)_3$, the differences in the molecular structures of their various electronic states are explained by the electronic structure analysis. On the basis of the result from CASPT2 and MS-CASPT2 calculations, we propose that the ground states of $Cr(CO)_2$ and $Cr(CO)_3$ are the $^5\Pi_g$ and $^1A_1$ states, respectively, addressing the ambiguity regarding their ground states. In addition, the multiconfigurational ab initio perturbation theory calculations reveal that (1) the energy gaps between the ground and first low-lying excited states of $Cr(CO)_2$ and $Cr(CO)_3$ are quite small and (2) the first low-lying excited states of $Cr(CO)_2$ and $Cr(CO)_3$ have the same spin multiplicities as the ground states of CrCO and $Cr(CO)_2$, respectively, which are the products of ligand dissociation. As a result, the apparent spin-forbidden dissociation of $Cr(CO)_2$ and $Cr(CO)_3$ into CrCO and $Cr(CO)_2$, respectively, are likely to be facilitated by thermal excitation of the ground states of $Cr(CO)_2$ and $Cr(CO)_3$ into their first low-lying excited states, which then actually undergoes the spin-allowed dissociation to the ground states of CrCO and $Cr(CO)_2$ with the same spin multiplicities.

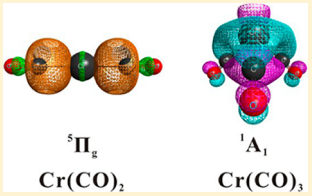

1. INTRODUCTION

Transition metal carbonyl complexes, ubiquitous building blocks in organometallic chemistry, play important roles in many chemical reactions and industrial processes.[1−5] Among them, $Cr(CO)_6$, which can be dissociated into various photoproducts upon irradiation, is a prototype of photodissociation dynamics of transition metal carbonyl complexes, and $Cr(CO)_n$ (n = 1−6) have been extensively investigated both theoretically[6−31] and experimentally.[32−44] As a means of investigating the photodissociation dynamics of the Cr carbonyl complexes, time-resolved diffraction can be used. In particular, ultrafast X-ray[45−62] diffraction and electron diffraction[63−67] are emerging experimental techniques to detect the molecular structure of the photoproducts (including transient intermediates) and the associated reaction pathways. To understand the photochemistry of $Cr(CO)_6$ by analyzing the data measured by ultrafast diffraction, theoretical information of the molecular structure of reaction intermediates is essential. As a theoretical tool for calculating molecular structures and estimating energetics of the intermediates involving transition metals, the density functional theory (DFT)[68,69] has been mainly used because it takes less computational time than post Hartree−Fock ab initio calculations and still treats electron correlation effect relatively well. Accordingly, various DFT functionals have been employed to study $Cr(CO)_n$ (n = 1−5) generated from photodissociation of $Cr(CO)_6$, giving the results comparable to the experimental ones.[21,22] The ground states of $Cr(CO)_6$, $Cr(CO)_5$, and $Cr(CO)_4$ calculated using various DFT methods are consistent with the experimental findings.[21] Also, the ground state of CrCO was identified as the $^7A'$ state, which is consistent with the experimental result, as well as the result from coupled cluster singles and doubles with perturbed triples (CCSD(T)),[70] a high-level single-reference ab initio method.[22]

In contrast to these Cr compounds, the ground states of $Cr(CO)_2$ and $Cr(CO)_3$ have not been clearly identified yet. The methods of DFT and CCSD (or CCSD(T)), which work well for other Cr carbonyl complexes, do not give the results consistent with the experimental findings for $Cr(CO)_2$ and $Cr(CO)_3$.[32,39,71] In addition, it was found that the ground state determined by geometry optimization varies depending on the computational method used for calculation.[21] For example, the ground state of $Cr(CO)_2$ was predicted to be $^5\Pi_g$ and $^7\Pi_u$ state by DFT and CCSD(T), respectively.[21,32] In contrast, a recent experiment using infrared spectroscopy on $Cr(CO)_2$ in the solid argon and neon matrix detected the $^5A_1$ state in C_{2v} symmetry, which is a bent structure, as the ground state.[32] For $Cr(CO)_3$, the predicted ground state also changes depending on the applied computational method. For example, generalized gradient approximation (GGA) DFT functionals and Møller−Plesset second-order

Received: January 31, 2013
Revised: April 14, 2013
Published: April 15, 2013

   dx.doi.org/10.1021/jp401128k | J. Phys. Chem. A 2013, 117, 3861−3868

perturbation theory (MP2) provided the $^1A_1$ state in C_{3v} symmetry as the ground state of $Cr(CO)_3$. By contrast, hybrid DFT and CCSD methods suggested that the $^5B_2$ state in C_{2v} symmetry lies lower in energy than the $^1A_1$ state.[21] Moreover, the reference wave functions of the single-reference methods are substantially contaminated in their spins according to the expectation value for square of the spin angular momentum, $\langle S^2 \rangle$. The spin contaminations of the single-reference ab initio methods such as MP2 and CCSD(T) are even worse than those of DFT.[21]

Considering high nondynamic correlation of Cr atom and the failure of DFT and single-reference ab initio methods for $Cr(CO)_2$ and $Cr(CO)_3$, the quantum chemical calculations based on the multireference wave function will be required to identify their ground states accurately. In addition, the electronic structure analysis is necessary for a better understanding of the nature of the bonding between metal and carbonyl. In the present work, we investigate the ground and low-lying excited states of $Cr(CO)_2$ and $Cr(CO)_3$ using the multireference ab initio methods, as well as DFT. We consider full valence orbitals of $Cr(CO)_2$ and $Cr(CO)_3$ in the multireference ab initio calculations and analyze their electronic structures to clarify their bonding nature. The calculated results are compared with the experimental results, and the discrepancy between the calculation and the experiment are discussed. In addition, the spin-forbidden reaction of $Cr(CO)_n$ ($n = 1-3$) is briefly discussed using the results of the calculation performed in this work.

2. COMPUTATIONAL DETAILS

We used complete active space self-consistent field (CASSCF)[72] theory to treat the nondynamic correlation effect. Ten and twelve active electrons were distributed in twelve and fifteen active orbitals for CASSCF calculations of $Cr(CO)_2$ and $Cr(CO)_3$, respectively. In other words, CAS(10,12) and CAS(12,15) were used for $Cr(CO)_2$ and $Cr(CO)_3$, respectively. These active orbitals contain five d and one s orbitals of Cr and all π^* and σ orbitals of CO molecules; the full valence orbitals of $Cr(CO)_2$ and $Cr(CO)_3$ were considered in CASSCF calculations. To consider the dynamic correlation effect, the multiconfigurational second-order perturbation theory, CASPT2[73,74] and multistate CASPT2 (MS-CASPT2)[75] methods were used. In all CASPT2 and MS-CASPT2 calculations, the standard IPEA shift value (0.25 au) was used for the zeroth-order Hamiltonian.

The CASPT2 was used for all states of $Cr(CO)_3$: $^1A_1$ ($^1A'$, the actual calculations were performed using C_s symmetry because the $^1A_1$ state in C_{3v} symmetry correlates to the $^1A'$ state in C_s symmetry), $^3B_1$, $^5B_2$, and $^7A_2''$ ($^7B_1$, the actual calculations were performed using C_{2v} symmetry because the $^7A_2''$ state in D_{3h} symmetry correlates to the $^7B_1$ state in C_{2v} symmetry). The $^3A_2$ and $^5A_1$ states of $Cr(CO)_2$ were also calculated using CASPT2 method. We note that, for the $^5\Pi_g$ and $^7\Pi_u$ states of $Cr(CO)_2$ with linear structure, the actual calculations were performed using C_2 symmetry to ensure the degeneracy of the states with $\Lambda \neq 0$. Therefore, for $^5\Pi_g$ and $^7\Pi_u$ states of $Cr(CO)_2$, we used state-average CASSCF to generate the reference wave functions and then MS-CASPT2 method. The 1s, 2s, and 2p electrons of Cr and 1s electrons of C and O were not correlated in all the CASPT2 and MS-CASPT2 calculations. In the (MS-)CASPT2 calculations, the quadruple [7s5p4d3f2g] and triple-ζ [4s3p2d1f] level of ANO-RCC[76] basis sets were used for Cr and other atoms (C and O), respectively, that is, ANO-RCC-QZ+TZ basis set. In all of the (MS-)CASPT2 calculations, Douglas-Kroll-Hess second-order (DKH2) method was used to treat the scalar relativistic effect.[77,78] The reliability of theoretical methods used for Cr in this work was already examined in a previous study;[79] CASPT2/ANO-RCC well reproduced the ionization potential and electron affinity of Cr atom with the discrepancy of less than 0.14 eV. We also checked the validity of the theoretical level for CO molecule by calculating the electron affinity (EA) of CO. The calculation of electron affinity of CO has been controversial because of discrepancy with the experimental result.[80] However, the EA calculated by CASPT2 is close to the value obtained from a high-level theoretical method (multireference configuration interaction, MRCI with very large basis sets). The full details of calculating the EA of CO are described in the Supporting Information. The geometry optimizations for $Cr(CO)_2$ and $Cr(CO)_3$ were performed using CASSCF, CASPT2, and MS-CASPT2 methods. To refine the energetics, we increased the level of calculation by changing the basis sets of C and O to quadruple-ζ (ANO-RCC-QZ) in the single-point energy calculations. In addition, to test the basis-set dependence, we also used the aug-cc-pVQZ (AVQZ)-DK,[81] [9s8p6d4f3g] (DK means contraction coefficients optimized for DKH calculation. The h functions were excluded to reduce the computation time.) and aug-cc-pVTZ (AVTZ)-DK, [5s4p3d2f] all-electron basis sets for Cr and other atoms (C and O), respectively, in the single-point (MS-)CASPT2 calculations. As a result, the performance of AVQZ+AVTZ-DK is almost the same as that of ANO-RCC-QZ+TZ. All CASSCF and (MS-)CASPT2 calculations were performed using the Molcas6.4 program.[82] For comparison, we also performed DFT and MP2 calculations for $Cr(CO)_2$ and $Cr(CO)_3$. The computational details of DFT and MP2 calculations are described in the Supporting Information.

3. RESULTS AND DISCUSSION

As mentioned above, we used CASSCF, CASPT2, MS-CASPT2, DFT, and MP2 methods for geometry optimization and energy calculation. We found that the result varies depending on the applied method. The molecular structures and energetics obtained by various methods are compared and discussed in detail in the Supporting Information, and here we focus on the result from the CASPT2 and MS-CASPT2 calculations, which give the most reliable results.

A. $Cr(CO)_2$. *Electronic Structure of $Cr(CO)_2$.* The molecular structures of $Cr(CO)_2$ are shown in Figure 1 and their optimized

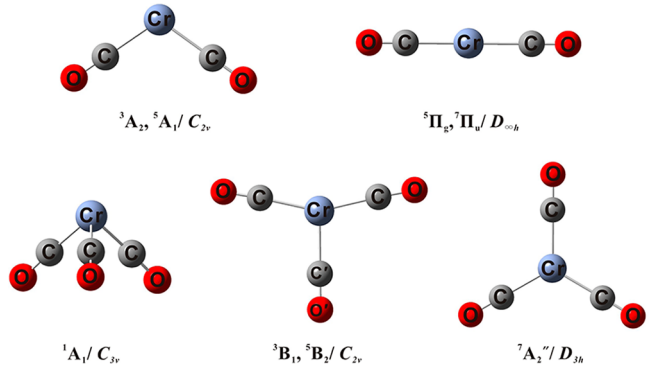

Figure 1. Molecular structures of $Cr(CO)_2$ and $Cr(CO)_3$ (molecular electronic state/molecular symmetry). The related optimized geometrical parameters of $Cr(CO)_2$ and $Cr(CO)_3$ are listed in Tables 1 and 2, respectively.

geometrical parameters are summarized in Table 1. The active orbitals of CAS(10,12) calculations for the $^3A_2$ and $^5A_1$ states

dx.doi.org/10.1021/jp401128k | J. Phys. Chem. A 2013, 117, 3861−3868

Table 1. Optimized Geometrical Parameters (Bond Lengths in Å and Bond Angles in Degree) and the Relative Energies,[b] ΔE (in kcal/mol), of the $^3A_2$, $^5A_1$, $^5\Pi_g$ (^5B), and $^7\Pi_u$ (^7B) States of $Cr(CO)_2$[a]

$Cr(CO)_2$	CAS(10,12)	(MS-)CASPT2[c]
	$^3A_2/C_{2v}$	
r(Cr−C)	1.842	1.823
r(C−O)	1.133	1.165
∠CCrC	76.8	72.4
∠CrCO	176.4	175.3
ΔE	0.2	16.3 (**16.7**) [16.5]
	$^5A_1/C_{2v}$	
r(Cr−C)	1.972	1.970
r(C−O)	1.121	1.150
∠CCrC	104.3	107.8
∠CrCO	175.2	176.2
ΔE	−3.6	10.5 (**9.4**) [10.6]
	$^5\Pi_g$ (^5B)/$D_{\infty h}$ (C_2)	
r(Cr−C)	2.005	1.958
r(C−O)	1.119	1.151
ΔE	0.0	0.0 (**0.0**) [0.0]
	$^7\Pi_u$ (^7B)/$D_{\infty h}$ (C_2)	
r(Cr−C)	2.077	2.006
r(C−O)	1.110	1.147
ΔE	−7.1	0.6 (**0.8**) [0.9]

[a]The related molecular structures of $Cr(CO)_2$ are shown in Figure 1. [b]Relative energies are with respect to the $^5\Pi_g$ state. [c]Values in parentheses were calculated by (MS-)CASPT2/ANO-RCC-QZ//(MS-)CASPT2/ANO-RCC-QZ+TZ. Values in square brackets were calculated by (MS-)CASPT2/AVQZ+AVTZ-DK//(MS-)CASPT2/ANO-RCC-QZ+TZ.

(bent structure) and for the $^5\Pi_g$ and $^7\Pi_u$ states (linear structure) are shown in Figures S1a and S1b in the Supporting Information, respectively. The order of MOs in the wave functions of the $^3A_2$ and $^5A_1$ states is $|a_{1(1)}a_{1(2)}a_{1(3)}a_{1(4)}a_{1(5)}b_{2(1)}b_{2(2)}b_{2(3)}a_{2(1)}a_{2(2)}b_{1(1)}b_{1(2)}\rangle$. An example of the electronic configuration is

$$|22 + 002 - 0 + 0 + 0\rangle = |a^2_{1(1)}a^2_{1(2)}a^1_{1(3)}a^0_{1(4)}a^0_{1(5)}b^2_{2(1)}b^1_{2(2)}b^0_{2(3)}a^1_{2(1)}a^0_{2(2)}b^1_{1(1)}b^0_{1(2)}\rangle$$

The "+" and "−" symbols mean the alpha and beta electrons, respectively. Note that there are twelve orbitals and ten electrons in total. The reference wave functions of the $^5A_1$ and $^3A_2$ states of $Cr(CO)_2$ from the CASPT2 calculations are shown in eqs 1 and 2, respectively.

$$|\Psi(^5A_1)\rangle = -0.904|22 + 002 + 0 + 0 + 0\rangle + 0.174|20 + 202 + 0 + 0 + 0\rangle + 0.155|2 + -+02 + 0 + 0 + 0\rangle + 0.110|2 + +-020 + +0 + 0\rangle... \quad (1)$$

$$|\Psi(^3A_2)\rangle = 0.891|22 + 00200 + 020\rangle - 0.147|22 + 00200 + 002\rangle - 0.132|20 + 20200 + 020\rangle - 0.108|2 + -+0200 + 020\rangle... \quad (2)$$

As can be seen in eqs 1 and 2, the major configuration of each wave function cover only ∼80% of the entire wave function for both $^5A_1$ and $^3A_2$ states, indicating multiconfigurational character of those states. Therefore, the single-reference method cannot properly describe either of the two states of $Cr(CO)_2$, and multireference ab initio methods need to be used as in this work.

The structures of $^3A_2$ and $^5A_1$ states are very different from each other (see Table 1). For example, the C−Cr−C angle of the $^3A_2$ state (72.4° at the CASPT2 level) is much smaller than that of the $^5A_1$ state (107.8°), which can be explained by the difference in their electronic configurations. The major electronic configuration of the $^3A_2$ state can be converted to that of the $^5A_1$ state by exciting one electron from $b_{1(1)}$ to $b_{2(2)}$. In other words, in the $^3A_2$ state, two electrons occupy the $b_{1(1)}$ orbital, resulting in strong overlap between the orbitals of two C atoms (see Figure S1a in the Supporting Information). This strong interaction between the C atoms accounts for the striking difference between the C−Cr−C angles of the $^3A_2$ and $^5A_1$ states. In addition, the second electronic configuration of the $^3A_2$ state supports the smaller C−Cr−C angle as well. The second electronic configuration of the $^3A_2$ state can be generated from the major configuration of the $^3A_2$ state by exciting two electrons from $b_{1(1)}$ to $b_{1(2)}$. As shown in Figure S1a in the Supporting Information, despite the antibonding between Cr and C atoms, the $b_{1(2)}$ orbital also shows strong overlap between two C atoms, thus contributing to the smaller C−Cr−C bond angle of the $^3A_2$ state.

Besides the C−Cr−C angle, the length of the Cr−C bond is different between the $^3A_2$ and $^5A_1$ states, that is, the Cr−C bond is longer in the $^5A_1$ state than in the $^3A_2$ state. In all of the minor electronic configurations of both $^3A_2$ and $^5A_1$ states, Cr−C π^* orbitals with antibonding character are occupied. The configurational interaction (CI) coefficients of the minor electronic configurations of the $^3A_2$ state are smaller than those of the $^5A_1$ state. As a result, those antibonding orbitals contribute less to the wave function of the $^3A_2$ state, thus leading to longer Cr−C bond lengths in the $^5A_1$ state than in the $^3A_2$ state.

The reference wave functions of the $^5\Pi_g$ and $^7\Pi_u$ states in MS-CASPT2 calculations are shown in eqs 3 and 4, respectively. The order of MOs in the wave functions of the two states is shown in Figure S1b in the Supporting Information.

$$|\Psi(^5\Pi_g)\rangle = -0.884|22 + ++02 + 0000\rangle - 0.211|22 + ++0 + +-000\rangle - 0.150|22 + ++00 + 2000\rangle - 0.132|22 + ++00 + 0020\rangle... \quad (3)$$

$$|\Psi(^7\Pi_u)\rangle = 0.964|22 + ++0 + +00 + 0\rangle + 0.111|220 + ++0 + +0 + 0\rangle - 0.101|22 + ++000 + ++0\rangle + 0.096|22 + ++0 + 0 + 00 + \rangle... \quad (4)$$

The $^5\Pi_g$ and $^7\Pi_u$ states are different in their structures, which can be also explained by the difference in their electronic configurations. The major electronic configuration (92.9%) of the $^7\Pi_u$ state can be prepared from the major configuration (78.1%) of the $^5\Pi_g$ state by exciting one electron from the Cr−C π orbital ($\pi_{g(1)}$, see Figure S1b in the Supporting Information) to the nonbonding orbital ($\pi_{u(1)}$). As a result, the $^7\Pi_u$ state has longer Cr−C bond than the $^5\Pi_g$ state.

Ground State of $Cr(CO)_2$. As shown in Table 1, the results from CASPT2 and MS-CASPT2 calculations show that the ground state of $Cr(CO)_2$ in the gas phase is the $^5\Pi_g$ state, which has a linear structure. (For comparison, CAS(10,12) predict the $^7\Pi_u$ state as the ground state of $Cr(CO)_2$. However, this result from the CASSCF calculation is not reliable because of the lack of dynamic correlation effect in CASSCF.) However, in a recent infrared experiment in Ar and Ne matrix environment, only the bent structure of $Cr(CO)_2$ with two C−O stretching bands was detected.[32] The authors of this study performed DFT calculations (BP86, one of GGA functional) to support the

dx.doi.org/10.1021/jp401128k | J. Phys. Chem. A 2013, 117, 3861−3868

experimental result, but their BP86 calculations showed that the $^5\Pi_g$ state (linear structure) is the ground state. To address this discrepancy, they considered two possibilities in that work.[32] First, if the theoretical level (BP86) used in that work is sufficiently high to calculate the electronic structure of $Cr(CO)_2$, the $^5\Pi_g$ state must be the ground state of $Cr(CO)_2$ in the gas phase, but the bent structure ($^5A_1$) might become more stable than the linear one ($^5\Pi_g$) in solid Ar and Ne due to interaction of the Cr center with the solid matrix. Second, if the bent structure observed in the experiment is indeed the ground state, more accurate calculation (than DFT) should give the $^5A_1$ state as the ground state. However, according to our calculated results using more accurate (MS-)CASPT2 (see Table 1) methods, the $^5\Pi_g$ state is still predicted to be the ground state of $Cr(CO)_2$, ruling out the second possibility. Also, the energy difference between the $^5A_1$ and $^5\Pi_g$ states calculated by (MS-)CASPT2 is 10.5 kcal/mol (see Table 1), which is acceptable as the interaction energy between metal and noble gas.[83] In addition, the energy gap between the $^5A_1$ and $^5\Pi_g$ states is further reduced (9.4 kcal/mol, see Table 1) with the refinement of energetics using quadruple-ζ level of basis sets for C and O atoms. Thus, we conclude that the ground state of $Cr(CO)_2$ is the $^5\Pi_g$ state in the gas phase. But, in the matrix environment, the interaction between metal center and noble gas can stabilize the bent structure ($^5A_1$), as was detected by infrared spectroscopy experiment.

First Low-Lying Excited State of $Cr(CO)_2$. Using transient absorption spectroscopy, Weitz et al. observed the C−O stretching mode of 1914 cm^{-1} frequency for photodissociation of $Cr(CO)_6$ in the gas phase.[39] This mode was assigned to the contribution from the linear structure of $Cr(CO)_2$, but its frequency is unexpectedly high. Later, Andrews et al. estimated that the C−O stretching frequency of the linear structure of $Cr(CO)_2$ in the gas phase should be about 1850 cm^{-1} in the ground state, and assigned the experimentally observed mode of 1914 cm^{-1} frequency to an excited state.[32,84] This ambiguity regarding the C−O stretching mode can be addressed using the calculated results presented in this work.

As shown in Table 1, from MS-CASPT2 calculations, the energy difference between the $^5\Pi_g$ and $^7\Pi_u$ states was determined to be only 0.6 kcal/mol. To further refine the energetics of the two states, we performed single-point MS-CASPT2 calculations with all quadruple-ζ basis sets and obtained the $^5\Pi_g$−$^7\Pi_u$ energy gap of 0.8 kcal/mol. This result confirms that the ground state of $Cr(CO)_2$ is the $^5\Pi_g$ state, but its first low-lying excited state, $^7\Pi_u$ state, lies slightly above the $^5\Pi_g$ state. This small energy gap between the $^5\Pi_g$ and $^7\Pi_u$ states indicates that the $^7\Pi_u$ state can coexist with the $^5\Pi_g$ state because their energy difference may be overcome readily by thermal excitation. In this case, it is possible that the C−O stretching mode of 1914 cm^{-1} frequency arises from the $^7\Pi_u$ state instead of the $^5\Pi_g$ state, which is in agreement with the assignment from the previous study.[32] We examined this possibility by calculating vibrational frequencies of each state and the detailed discussion is presented in the Supporting Information. According to the results, we can conclude that 1914 cm^{-1} mode observed in the transient absorption experiment[39] is not from the C−O stretching of the $^5\Pi_g$ state but from the $^7\Pi_u$ state, supporting the assignment by Andrews et al.[32] According to these results, to address nearly degenerate states, such as the $^5\Pi_g$ and $^7\Pi_u$ states of $Cr(CO)_2$ and calculate the electronic states of linear molecules ($\Lambda \neq 0$) properly, multiconfigurational method including dynamic electron correlation effect, for example CASPT2, is necessary.

B. $Cr(CO)_3$. *Electronic Structure of $Cr(CO)_3$.* The molecular structures of $Cr(CO)_3$ are shown in Figure 1 and their optimized geometrical parameters are summarized in Table 2. The active orbitals of CAS(12,15) calculations for the $^1A_1$ ($^1A'$) state and the $^3B_1$, $^5B_2$, and $^7A_2''$ ($^7B_1$) states are depicted in Figures S2a and S2b in the Supporting Information, respectively. The reference wave function of the $^1A_1$ ($^1A'$) state of $Cr(CO)_3$ is shown in eq 5 and the order of MOs in the wave function is shown in Figure S2a in the Supporting Information.

Table 2. Optimized Geometrical Parameters (Bond Lengths in Å and Bond Angles in Degree) and the Relative Energies,[b] ΔE (in kcal/mol), of the $^1A_1$ ($^1A'$), $^3B_1$, $^5B_2$, and $^7A_2''$ ($^7B_1$) States of $Cr(CO)_3$[a]

$Cr(CO)_3$	CAS(12,15)	CASPT2[c]
	$^1A_1$ ($^1A'$)/C_{3v} (C_s)	
r(Cr−C)	1.839	1.806
r(C−O)	1.126	1.159
∠CCrC	88.4	85.7
∠CrCO	178.0	176.2
ΔE	0.0	0.0 (**0.0**) [0.0]
	$^3B_1$/C_{2v}	
r(Cr−C′)	1.940	1.894
r(C′−O′)	1.113	1.145
r(Cr−C)	1.931	1.904
r(C−O)	1.121	1.156
∠CCrC	179.3	177.9
∠C′CrC	89.6	88.9
∠CrCO	176.9	175.3
ΔE	18.6	8.9 (**8.5**) [8.5]
	$^5B_2$/C_{2v}	
r(Cr−C′)	1.988	1.999
r(C′−O′)	1.118	1.148
r(Cr−C)	2.027	2.005
r(C−O)	1.110	1.139
∠CCrC	155.1	159.5
∠C′CrC	102.4	100.2
∠CrCO	178.5	176.2
ΔE	12.0	1.9 (**4.8**) [2.0]
	$^7A_2''$ ($^7B_1$)/D_{3h} (C_{2v})	
r(Cr−C)	2.088	2.015
r(C−O)	1.106	1.142
ΔE	11.6	8.9 (**8.4**) [9.9]

[a]The related molecular structures of $Cr(CO)_3$ are shown in Figure 1. [b]Relative energies are with respect to the $^1A_1$ state. [c]Values in parentheses were calculated by CASPT2/ANO-RCC-QZ//CASPT2/ANO-RCC-QZ+TZ. Values in square brackets were calculated by CASPT2/AVQZ+AVTZ-DK//CASPT2/ANO-RCC-QZ+TZ.

$$|\Psi(^1A')\rangle = 0.896|222200000220000\rangle + 0.107|22 + 20 - 0002 + -000\rangle - 0.105|220202000220000\rangle - 0.102|222 + -00002 + -000\rangle... \quad (5)$$

Note that there are fifteen orbitals and twelve electrons in total. As shown in eq 5, in the major electronic configuration, all of the electrons occupy Cr−C σ and π orbitals that have strong binding character. As a result, the $^1A_1$ ($^1A'$) state has the shortest Cr−C bond length (in the CASPT2 calculations) among the states investigated in this work.

dx.doi.org/10.1021/jp401128k | J. Phys. Chem. A 2013, 117, 3861−3868

The reference wave functions of the $^3B_1$, $^5B_2$, and $^7A_2''$ ($^7B_1$) states are as follows:

$$|\Psi(^3B_1)\rangle = 0.891|22 + 000220020 + 00\rangle - 0.115|22 + 000220002 + 00\rangle - 0.115|22 + 000202020 + 00\rangle... \quad (6)$$

$$|\Psi(^5B_2)\rangle = 0.907|22 + +002200 + 0 + 00\rangle - 0.148|22 + +002020 + 0 + 00\rangle - 0.102|22 + 0 + 02 + -0 + 0 + 00\rangle... \quad (7)$$

$$|\Psi(^7B_1)\rangle = -0.951|22 + +002 + 00 + 0 + 0 + \rangle - 0.079|22 + 0 + 02 + 000 + +0 + \rangle... \quad (8)$$

The order of MOs in the wave functions is shown in Figure S2b in the Supporting Information. The molecular structures of these three states ($^3B_1$, $^5B_2$, and $^7B_1$) have different C′−Cr−C bond angles, 88.9°, 100.2°, and 120.0°, respectively, indicating that the bond angle increases as the spin multiplicity increases. As shown in eq 7, the major electronic configuration of the $^5B_2$ state can be prepared from the major electronic configuration of the $^3B_1$ state by exciting one electron from the $a_{2(1)}$ to $a_{1(4)}$. Since the $a_{1(4)}$ orbital has a nodal plane-like structure between Cr−C′ and Cr−C bonds (that is, the phases of the MO's are different, see Figure S2b in the Supporting Information), the occupation of the $a_{1(4)}$ orbital leads to unfavorable interaction, thereby increasing the C′−Cr−C bond angle in the $^5B_2$ state. In contrast, the major electronic configuration of the $^7A_2''$ ($^7B_1$) state can be prepared from the major electronic configuration of the $^5B_2$ state by exciting one electron from the $b_{2(2)}$ to $b_{1(3)}$. In the $b_{2(2)}$ orbital, there exists strong interaction (Cr−C π orbitals) between d orbital lying in the molecular plane and π orbital of CO (see Figure S2b in the Supporting Information). Therefore, the $^7A_2''$ ($^7B_1$) state, which has one less electron in the $b_{2(2)}$ orbital of strong binding character, is likely to have a larger C′−Cr−C bond angle (120°) than the $^5B_2$ state.

As can be seen in Table 2, the Cr−C bond length also increases as the spin multiplicity increases. In the major electronic configuration of the $^3B_1$ state, two electrons occupy the $a_{2(1)}$ orbital, which is a Cr−C π-bonding orbital, resulting in shorter Cr−C distance than in other states. In addition, the minor electronic configurations of the $^3B_1$ and $^5B_2$ states support the bond elongation in the $^5B_2$ state as well. In all of the minor electronic configurations of the $^3B_1$ and $^5B_2$ states, the Cr−C π-antibonding orbitals are occupied, as can be seen in eqs 6 and 7. Since the contribution of minor electronic configurations is slightly larger in the $^5B_2$ state (3.2%) than in the $^3B_1$ state (2.6%), the Cr−C bond in the $^5B_2$ state is likely to be longer than in the $^3B_1$ state. For the $^7A_2''$ ($^7B_1$) state, as mentioned above, only one electron occupies the $b_{2(2)}$ orbital unlike in other states ($^3B_1$ and $^5B_2$) that have two electrons in the $b_{2(2)}$ orbital. Moreover, the CI coefficient (−0.951) of the major electronic configuration of the $^7A_2''$ ($^7B_1$) state is larger than that of other states. This one-electron occupation of the $b_{2(2)}$ orbital with strong binding character leads to further elongation of the Cr−C bond length in the $^7A_2''$ ($^7B_1$) state. Thus, the elongation of the Cr−C bond with the increase of spin multiplicity is well accounted for by the electronic structure of each state.

Ground State of $Cr(CO)_3$. From CASPT2 calculations based on CAS(12,15), the ground state of $Cr(CO)_3$ is determined to be the $^1A_1$ ($^1A'$) state, which lies lower in energy by 1.9 kcal/mol than the $^5B_2$ state. In addition, the refinement using quadruple-ζ basis sets for C and O also provides the $^1A_1$ ($^1A'$) as the ground state of $Cr(CO)_3$ by 4.8 kcal/mol. This assignment is consistent with the experiment.[39,71] In a previous study, the $^5B_2$ state calculated by CCSD method lies lower in energy by 13.0 kcal/mol than the $^1A_1$ ($^1A'$) state.[21] All these results imply that the consideration of multiconfigurational character is crucial to obtain correct energy ordering of $Cr(CO)_3$, and therefore, the use of multiconfigurational method is essential to address nearly degenerate electronic states of $Cr(CO)_3$ as for $Cr(CO)_2$.

C. Spin-Forbidden Reactions of $Cr(CO)_2$ and $Cr(CO)_3$. The sequential dissociation (thermolysis) of CO ligands from $Cr(CO)_6$ to $Cr(CO)_3$ are spin-allowed reactions because the ground states of $Cr(CO)_n$ (n = 3−6) are all singlet states and the CO ($^1\Sigma^+$) ligand is singlet.[21,39] In contrast, the dissociation reactions (1) from the ground state of $Cr(CO)_3$ to the ground state of $Cr(CO)_2$ and (2) from the ground state of $Cr(CO)_2$ to the ground state of CrCO are all spin-forbidden reactions because the ground states of $Cr(CO)_3$, $Cr(CO)_2$, and CrCO are singlet, quintet, and septet, respectively. A similar spin-forbidden reaction, $Fe(CO)_4 + CO \rightarrow Fe(CO)_5$, and their origin were previously studied,[85,86] but the origin of the spin-forbidden reactions of $Cr(CO)_n$ (n = 1−3) has not been clearly explained so far.

The calculation results presented in this work provide insight to these processes. As mentioned in the previous sections, the energy differences between the ground and the first excited states of $Cr(CO)_2$ and $Cr(CO)_3$ are only 0.8 kcal/mol (MS-CASPT2/ANO-RCC-QZ//MS-CASPT2/ANO-RCC-QZ+TZ, $^5\Pi_g$ and $^7\Pi_u$) and 4.8 kcal/mol (CASPT2/ANO-RCC-QZ//CASPT2/ANO-RCC-QZ+TZ, $^1A_1$ and $^5B_2$), respectively. These energy differences are very small and can be readily overcome by thermal energy. In addition, the first low-lying excited states of $Cr(CO)_2$ ($^7\Pi_u$) and $Cr(CO)_3$ ($^5B_2$) have the same spin multiplicities as the ground states of their ligand-dissociation products, CrCO ($^7A'$) and $Cr(CO)_2$ ($^5\Pi_g$), respectively. Therefore, the first low-lying excited states of $Cr(CO)_2$ and $Cr(CO)_3$ are easily populated by thermal energy and then undergo spin-allowed reactions to the ground states of CrCO and $Cr(CO)_2$, respectively. In other words, the apparent spin-forbidden reaction of $Cr(CO)_n$ (n = 1−3) becomes a spin-allowed reaction because of the small energy gap between the ground and the first excited states. On the basis of this scenario, we propose the reaction mechanism of the apparent spin-forbidden dissociation of $Cr(CO)_2$ into CrCO as follows: the ground state of $Cr(CO)_2$ (quintet) → the first excited state of $Cr(CO)_2$ (septet) → the ground state of CrCO (septet) + CO, where the second step is actually spin-allowed dissociation.

Another possible origin of the spin-forbidden reaction is spin−orbit coupling (SOC); different spin multiplicity states can be mixed by SOC at a specific molecular structure, which is called intersystem crossing (ISC) point. This mechanism was used to account for the spin-forbidden reaction of $Fe(CO)_4$.[85,86] However, since SOC is rather weak for the first-row transition metal, a crossing probability between different spin multiplicity states is very low. In addition, the wave packet should be close to an ISC point. Therefore, spin-forbidden reaction mediated by SOC is likely to be a minor reaction channel in the spin-forbidden reactions of $Cr(CO)_n$ (n = 1−3).

The metal complexes $Cr(CO)_3$ and $Cr(CO)_2$ presented in this work have uniquely small energy gap between the ground and the first excited states. In the case of $Fe(CO)_4$, the energy gap is ∼8 kcal/mol[85] and cannot be easily overcome by thermal energy. Thus, this apparent spin-forbidden reaction of $Cr(CO)_n$ (n = 1−3) occurs by a spin-allowed reaction, which is driven by thermal population of the first low-lying excited state.

dx.doi.org/10.1021/jp401128k | J. Phys. Chem. A 2013, 117, 3861−3868

4. CONCLUSION

The multireference ab initio calculations were carried out to identify the ground and low-lying excited states of unsaturated chromium carbonyls, $Cr(CO)_2$ and $Cr(CO)_3$. The analysis of electronic structures clearly explains the structural differences among the electronic states of $Cr(CO)_2$ and $Cr(CO)_3$. The CASPT2 and MS-CASPT2 calculations show that the ground state of $Cr(CO)_2$ is the $^5\Pi_g$ state in the gas phase. The first low-lying excited state of $Cr(CO)_2$ is the $^7\Pi_u$ state that lies higher in energy by only 0.8 kcal/mol than the $^5\Pi_g$ state; therefore, both $^5\Pi_g$ and $^7\Pi_u$ states can coexist. From this result, we suggest that the unexpectedly high frequency of the C−O stretching mode observed in the transient absorption experiment in the gas phase can be ascribed to the vibrational frequency of $^7\Pi_u$ state, which can be easily populated due to the small energy gap from the ground state. Thus, the calculated results in this work clearly address the discrepancy between the calculation and experiment regarding the identity of the ground states. For $Cr(CO)_3$, CASPT2 calculations show that the ground state is the $^1A_1$ state of C_{3v} structure, which is consistent with the experimental finding. The first low-lying excited states of $Cr(CO)_2$ and $Cr(CO)_3$ are the $^7\Pi_u$ and $^5B_2$ states, respectively, which have the same spin multiplicities as the ground states of their corresponding ligand-dissociation products, CrCO ($^7A'$) and $Cr(CO)_2$ ($^5\Pi_g$), respectively. In addition, the energy differences between the ground state and the first low-lying excited states are only 0.8 and 4.8 kcal/mol for $Cr(CO)_2$ and $Cr(CO)_3$, respectively. These small energy differences are likely to facilitate the apparent spin-forbidden reaction of the ground states of $Cr(CO)_2$ and $Cr(CO)_3$ via the low-lying excited states of $Cr(CO)_2$ and $Cr(CO)_3$ generated by thermal excitation.

■ ASSOCIATED CONTENT

Supporting Information

Full details of calculations of EA of CO (Table S1), the computational details of the DFT and MP2 (single-reference methods) calculations, the optimized geometrical parameters, $\langle S^2 \rangle$ values, the relative energies of all the states of $Cr(CO)_2$ and $Cr(CO)_3$ calculated using DFT and MP2 (Tables S2 and S3, respectively), the comparison of the molecular structure and energetics obtained by DFT, MP2, and CASSCF, the detailed discussion of CO stretching frequency of the $^7\Pi_u$ state, and the active orbitals of $Cr(CO)_2$ and $Cr(CO)_3$ (Figures S1 and S2, respectively). This material is available free of charge via the Internet at http://pubs.acs.org.

■ AUTHOR INFORMATION

Corresponding Author

*E-mail: joonghankim@catholic.ac.kr (J.K.); hyotcherl.ihee@kaist.ac.kr (H.I.).

Notes

The authors declare no competing financial interest.

■ ACKNOWLEDGMENTS

This work was supported by the Catholic University of Korea, Research Fund, 2012. This work was supported by the Research Center Program (CA1201) of IBS (Institute for Basic Science) in Korea.

■ REFERENCES

(1) Cotton, F. A.; Wilkinson, G.; Murillo, C. A.; Bochmann, M. *Advanced Inorganic Chemistry*, 6th ed.; Wiley: New York, 1999.

(2) Ellis, J. E. Highly Reduced Metal Carbonyl Anions: Synthesis, Characterization, and Chemical Properties. *Adv. Organomet. Chem.* **1990**, *31*, 1−51.

(3) Hoffmann, R. Building Bridges between Inorganic and Organic−Chemistry (Nobel Lecture). *Angew. Chem., Int. Ed. Engl.* **1982**, *21*, 711−724.

(4) Muetterties, E. L.; Stein, J. Mechanistic Features of Catalytic Carbon-Monoxide Hydrogenation Reactions. *Chem. Rev.* **1979**, *79*, 479−490.

(5) Tumas, W.; Gitlin, B.; Rosan, A. M.; Yardley, J. T. Olefin Rearrangement Resulting from the Gas-Phase Krypton Fluoride Laser Photolysis of Chromium Hexacarbonyl. *J. Am. Chem. Soc.* **1982**, *104*, 55−59.

(6) Barnes, L. A.; Rosi, M.; Bauschlicher, C. W., Jr. An Ab Initio Study of $Fe(CO)_n$, n = 1,5, and $Cr(CO)_6$. *J. Chem. Phys.* **1991**, *94*, 2031−2039.

(7) Fan, L.; Ziegler, T. Optimization of Molecular Structures by Self-Consistent and Nonlocal Density-Functional Theory. *J. Chem. Phys.* **1991**, *95*, 7401−7408.

(8) Fan, L.; Ziegler, T. Application of Density Functional Theory to Infrared Absorption Intensity Calculations on Transition-Metal Carbonyls. *J. Phys. Chem.* **1992**, *96*, 6937−6941.

(9) Lin, Z.; Hall, M. B. Theoretical Studies of Inorganic and Organometallic Reaction Mechanisms. 5. Substitution Reactions of 17- and 18-Electron Transition-Metal Hexacarbonyl Complexes. *Inorg. Chem.* **1992**, *31*, 2791−2797.

(10) Barnes, L. A.; Liu, B.; Lindh, R. Structure and Energetics of $Cr(CO)_6$ and $Cr(CO)_5$. *J. Chem. Phys.* **1993**, *98*, 3978−3989.

(11) Davidson, E. R.; Kunze, K. L.; Machado, F. B. C.; Chakravorty, S. J. The Transition Metal-Carbonyl Bond. *Acc. Chem. Res.* **1993**, *26*, 628−635.

(12) Li, J.; Schreckenbach, G.; Ziegler, T. First Bond Dissociation Energy of $M(CO)_6$ (M = Cr, Mo, W) Revisited: The Performance of Density Functional Theory and the Influence of Relativistic Effects. *J. Phys. Chem.* **1994**, *98*, 4838−4841.

(13) Delley, B.; Wrinn, M.; Lüthi, H. P. Binding Energies, Molecular Structures, and Vibrational Frequencies of Transition Metal Carbonyls Using Density Functional Theory with Gradient Corrections. *J. Chem. Phys.* **1994**, *100*, 5785−5791.

(14) Berces, A.; Ziegler, T. Harmonic Force Fields and Vibrational Frequencies of Benzene, Dibenzene-Chromium, Benzene-Chromium Tricarbonyl, and Chromium-Hexacarbonyl. A Density Functional Study. *J. Phys. Chem.* **1994**, *98*, 13233−13242.

(15) Ehlers, A. W.; Frenking, G. Structures and Bond Energies of the Transition Metal Hexacarbonyls $M(CO)_6$ (M = Cr, Mo, W). A Theoretical Study. *J. Am. Chem. Soc.* **1994**, *116*, 1514−1520.

(16) Dapprich, S.; Pidun, U.; Ehlers, A. W.; Frenking, G. The Calculation of Bond Dissociation Energies of Transition Metal Complexes Using Isostructural Reactions. *Chem. Phys. Lett.* **1995**, *242*, 521−526.

(17) Li, J.; Schreckenbach, G.; Ziegler, T. A Reassessment of the First Metal-Carbonyl Dissociation Energy in $M(CO)_4$ (M = Ni, Pd, Pt), $M(CO)_5$ (M = Fe, Ru, Os), and $M(CO)_6$ (M = Cr, Mo, W) by a Quasirelativistic Density Functional Method. *J. Am. Chem. Soc.* **1995**, *117*, 486−494.

(18) Jonas, V.; Thiel, W. Theoretical Study of the Vibrational Spectra of the Transition Metal Carbonyls $M(CO)_6$ [M = Cr, Mo, W], $M(CO)_5$ [M = Fe, Ru, Os], and $M(CO)_4$ [M = Ni, Pd, Pt]. *J. Chem. Phys.* **1995**, *102*, 8474−8484.

(19) Ehlers, A. W.; Ruiz-Morales, Y.; Baerends, E. J.; Ziegler, T. Dissociation Energies, Vibrational Frequencies, and ^{13}C NMR Chemical Shifts of the 18-Electron Species $[M(CO)_6]^n$ (M = Hf−Ir, Mo, Tc, Ru, Cr, Mn, Fe). A Density Functional Study. *Inorg. Chem.* **1997**, *36*, 5031−5036.

(20) Koukounas, C.; Kardahakis, S.; Mavridis, A. Electronic and geometric structure of the 3d-transition metal monocarbonyls MCO, M = Sc, Ti, V, and Cr. *J. Chem. Phys.* **2005**, *123*, 074327.

(21) Kim, J.; Kim, T. K.; Kim, J.; Lee, Y. S.; Ihee, H. Density Functional and Ab Initio Study of $Cr(CO)_n$ (n = 1−6) Complexes. *J. Phys. Chem. A* **2007**, *111*, 4697−4710.

(22) Kim, J.; Lee, Y. S.; Ihee, H. Density Functional and Ab Initio Studies on Structures and Energies of the Ground State of CrCO. *Int. J. Quantum Chem.* **2007**, *107*, 458−463.
(23) Machado, F. B. C.; Davidson, E. R. Binding Energy of Chromium Hexacarbonyl. 2. Revisited with Correlation Effects. *J. Phys. Chem.* **1993**, *97*, 4397−4403.
(24) Persson, B. J.; Roos, B. O.; Pierloot, K. A Theoretical Study of the Chemical Bonding in $M(CO)_x$ (M = Cr, Fe, and Ni). *J. Chem. Phys.* **1994**, *101*, 6810−6821.
(25) Rolke, J.; Zheng, Y.; Brion, C. E.; Chakravorty, S. J.; Davidson, E. R.; McCarthy, I. E. Imaging of the HOMO Electron Density in $Cr(CO)_6$, $Mo(CO)_6$, and $W(CO)_6$ by Electron Momentum Spectroscopy: A Comparison with Hartree-Fock and DFT Calculations. *Chem. Phys.* **1997**, *215*, 191−205.
(26) Rosa, A.; Baerends, E. J.; van Gisbergen, S. J. A.; van Lenthe, E.; Groeneveld, J. A.; Snijders, J. G. Electronic Spectra of $M(CO)_6$ (M = Cr, Mo, W) Revisited by a Relativistic TDDFT Approach. *J. Am. Chem. Soc.* **1999**, *121*, 10356−10365.
(27) Rosa, A.; Ehlers, A. W.; Baerends, E. J.; Snijders, J. G.; Velde, G. t. Basis Set Effects in Density Functional Calculations on the Metal−Ligand and Metal−Metal Bonds of $Cr(CO)_5$−CO and $(CO)_5Mn$−$Mn(CO)_5$. *J. Phys. Chem.* **1996**, *100*, 5690−5696.
(28) Sosa, C.; Andzelm, J.; Elkin, B. C.; Wimmer, E.; Dobbs, K. D.; Dixon, D. A. A Local Density Functional Study of the Structure and Vibrational Frequencies of Molecular Transition-Metal Compounds. *J. Phys. Chem.* **1992**, *96*, 6630−6636.
(29) Spears, K. G. Density Functional Study of Geometry and Vibrational Spectra for the Isoelectronic $V(CO)_6^-$ and $Cr(CO)_6$ Molecules. *J. Phys. Chem. A* **1997**, *101*, 6273−6279.
(30) van Wüllen, C. A Relativistic Kohn−Sham Density Functional Procedure by Means of Direct Perturbation Theory. II. Application to the Molecular Structure and Bond Dissociation Energies of Transition Metal Carbonyls and Related Complexes. *J. Chem. Phys.* **1996**, *105*, 5485−5493.
(31) Ziegler, T.; Tschinke, V.; Ursenbach, C. Thermal Stability and Kinetic Lability of the Metal Carbonyl Bond. A Theoretical Study on $M(CO)_6$ (M = Chromium, Molybdenum, Tungsten), $M(CO)_5$ (M = Iron, Ruthenium, Osmium), and $M(CO)_4$ (M = Nickel, Palladium, Platinum). *J. Am. Chem. Soc.* **1987**, *109*, 4825−4837.
(32) Andrews, L.; Zhou, M. F.; Gutsev, G. L.; Wang, X. F. Reactions of Laser-Ablated Chromium Atoms, Cations, and Electrons with CO in Excess Argon and Neon: Infrared Spectra and Density Functional Calculations on Neutral and Charged Unsaturated Chromium Carbonyls. *J. Phys. Chem. A* **2003**, *107*, 561−569.
(33) Church, S. P.; Grevels, F.; Hermann, H.; Schaffner, K. Structures and Kinetics of Pentacarbonylchromium and Pentacarbonylchromium Monohydrate. *Inorg. Chem.* **1985**, *24*, 418−422.
(34) Fletcher, T. R.; Rosenfeld, R. N. Recombination of $Cr(CO)_n$ with CO: Kinetics and Bond Dissociation Energies. *J. Am. Chem. Soc.* **1988**, *110*, 2097−2101.
(35) Gutmann, M.; Dickebohm, M. S.; Janello, J. M. Ultrafast Dynamics of Transition Metal Carbonyls. 3. Intracluster Chemistry in $[Cr(CO)_6]_n$. *J. Phys. Chem. A* **1999**, *103*, 2580−2591.
(36) Gutmann, M.; Janello, J. M.; Dickebohm, M. S.; Grossekathofer, M.; Lindener-Roenneke, J. Ultrafast Dynamics of Transition Metal Carbonyls: Photodissociation of $Cr(CO)_6$ and $Cr(CO)_6{\cdot}(CH_3OH)_n$ Heteroclusters at 280 nm. *J. Phys. Chem. A* **1998**, *102*, 4138−4147.
(37) Lewis, K. E.; Golden, D. M.; Smith, G. P. Organometallic Bond Dissociation Energies: Laser Pyrolysis of Iron Pentacarbonyl, Chromium Hexacarbonyl, Molybdenum Hexacarbonyl, and Tungsten Hexacarbonyl. *J. Am. Chem. Soc.* **1984**, *106*, 3905−3912.
(38) Perutz, R. N.; Turner, J. J. Photochemistry of the Group 6 Hexacarbonyls in Low-Temperature Matrices. III. Interaction of the Pentacarbonyls with Noble Gases and Other Matrices. *J. Am. Chem. Soc.* **1975**, *97*, 4791−4800.
(39) Seder, T. A.; Church, S. P.; Weitz, E. Wavelength dependence of excimer laser photolysis of $Cr(CO)_6$ in the gas phase. A study of the infrared spectroscopy and reactions of the $Cr(CO)_x$ (x = 5, 4, 3, 2) Fragments. *J. Am. Chem. Soc.* **1986**, *108*, 4721−4728.
(40) Trushin, S. A.; Fuss, W.; Schmid, W. E.; Kompa, K. L. Femtosecond Dynamics and Vibrational Coherence in Gas-Phase Ultraviolet Photodecomposition of $Cr(CO)_6$. *J. Phys. Chem. A* **1998**, *102*, 4129−4137.
(41) Trushin, S. A.; Sugawara, K.; Takeo, H. Observation of CrCO in the 5 μm Multiphoton Decomposition of $Cr(CO)_6$. *Chem. Phys. Lett.* **1997**, *267*, 573−579.
(42) Venkataraman, B.; Hou, H.; Zhang, Z.; Chen, S.; Bandukwalla, G.; Vernon, M. A Molecular Beam Study of the One, Two, and Three Photon Photodissociation Mechanism of the Group VIB (Cr, Mo, W) Hexacarbonyls at 248 nm. *J. Chem. Phys.* **1990**, *92*, 5338−5362.
(43) Weitz, E. Transient Infrared-Spectroscopy as a Probe of Coordinatively Unsaturated Metal-Carbonyls in the Gas-Phase. *J. Phys. Chem.* **1994**, *98*, 11256−11264.
(44) Willey, K. F.; Brummel, C. L.; Winograd, N. Photoionization Mechanisms for $Cr(CO)_6$ Using High Intensity Laser Pulses in the Near-IR. *Chem. Phys. Lett.* **1997**, *267*, 359−364.
(45) Ihee, H.; Lorenc, M.; Kim, T. K.; Kong, Q. Y.; Cammarata, M.; Lee, J. H.; Bratos, S.; Wulff, M. Ultrafast X-ray Diffraction of Transient Molecular Structures in Solution. *Science* **2005**, *309*, 1223−1227.
(46) Davidsson, J.; Poulsen, J.; Cammarata, M.; Georgiou, P.; Wouts, R.; Katona, G.; Jacobson, F.; Plech, A.; Wulff, M.; Nyman, G.; Neutze, R. Structural Determination of a Transient Isomer of CH_2I_2 by Picosecond X-Ray Diffraction. *Phys. Rev. Lett.* **2005**, *94*, 245503.
(47) Plech, A.; Cerna, R.; Kotaidis, V.; Hudert, F.; Bartels, A.; Dekorsy, T. A Surface Phase Transition of Supported Gold Nanoparticles. *Nano Lett.* **2007**, *7*, 1026−1031.
(48) Cammarata, M.; Levantino, M.; Schotte, F.; Anfinrud, P. A.; Ewald, F.; Choi, J.; Cupane, A.; Wulff, M.; Ihee, H. Tracking the Structural Dynamics of Proteins in Solution Using Time-Resolved Wide-Angle X-ray Scattering. *Nat. Meth.* **2008**, *5*, 881−886.
(49) Ihee, H. Visualizing Solution-Phase Reaction Dynamics with Time-Resolved X-ray Liquidography. *Acc. Chem. Res.* **2009**, *42*, 356−366.
(50) Kim, T. K.; Lee, J. H.; Wulff, M.; Kong, Q.; Ihee, H. Spatiotemporal Kinetics in Solution Studied by Time-Resolved X-Ray Liquidography (Solution Scattering). *ChemPhysChem* **2009**, *10*, 1958−1980.
(51) Christensen, M.; Haldrup, K.; Bechgaard, K.; Feidenhans'l, R.; Kong, Q.; Cammarata, M.; Russo, M. L.; Wulff, M.; Harrit, N.; Nielsen, M. M. Time-Resolved X-ray Scattering of an Electronically Excited State in Solution. Structure of the $^3A_{2u}$ State of Tetrakis-μ-pyrophosphitodiplatinate(II). *J. Am. Chem. Soc.* **2009**, *131*, 502−508.
(52) Haldrup, K.; Christensen, M.; Cammarata, M.; Kong, Q.; Wulff, M.; Mariager, S. O.; Bechgaard, K.; Feidenhans'l, R.; Harrit, N.; Nielsen, M. M. Structural Tracking of a Bimolecular Reaction in Solution by Time-Resolved X-Ray Scattering. *Angew. Chem., Int. Ed.* **2009**, *48*, 4180−4184.
(53) Vincent, J.; Andersson, M.; Eklund, M.; Wohri, A. B.; Odelius, M.; Malmerberg, E.; Kong, Q.; Wulff, M.; Neutze, R.; Davidsson, J. Solvent Dependent Structural Perturbations of Chemical Reaction Intermediates Visualized by Time-Resolved X-ray Diffraction. *J. Chem. Phys.* **2009**, *130*, 154502.
(54) Ihee, H.; Wulff, M.; Kim, J.; Adachi, S. Ultrafast X-ray Scattering: Structural Dynamics from Diatomic to Protein Molecules. *Int. Rev. Phys. Chem.* **2010**, *29*, 453−520.
(55) Jun, S.; Lee, J. H.; Kim, J.; Kim, J.; Kim, K. H.; Kong, Q.; Kim, T. K.; Russo, M. L.; Wulff, M.; Ihee, H. Photochemistry of $HgBr_2$ in Methanol Investigated Using Time-Resolved X-ray Liquidography. *Phys. Chem. Chem. Phys.* **2010**, *12*, 11536−11547.
(56) Kong, Q.; Lee, J. H.; Kim, K. H.; Kim, J.; Wulff, M.; Ihee, H.; Koch, M. H. J. Ultrafast X-ray Solution Scattering Reveals Different Reaction Pathways in the Photolysis of Triruthenium Dodecacarbonyl ($Ru_3(CO)_{12}$) after Ultraviolet and Visible Excitation. *J. Am. Chem. Soc.* **2010**, *132*, 2600−2607.
(57) Christensen, M.; Haldrup, K.; Kjaer, K. S.; Cammarata, M.; Wulff, M.; Bechgaard, K.; Weihe, H.; Harrit, N.; Nielsen, M. M. Structure of a Short-Lived Excited State Trinuclear Ag−Pt−Pt Complex in Aqueous

Solution by Time-Resolved X-ray Scattering. *Phys. Chem. Chem. Phys.* **2010**, *12*, 6921−6923.
(58) Ibrahimkutty, S.; Kim, J.; Cammarata, M.; Ewald, F.; Choi, J.; Ihee, H.; Plech, A. Ultrafast Structural Dynamics of the Photocleavage of Protein Hybrid Nanoparticles. *ACS Nano* **2011**, *5*, 3788−3794.
(59) Malmerberg, E.; Omran, Z.; Hub, J. S.; Li, X.; Katona, G.; Westenhoff, S.; Johansson, L. C.; Andersson, M.; Cammarata, M.; Wulff, M.; van der Spoel, D.; Davidsson, J.; Specht, A.; Neutze, R. Time-Resolved WAXS Reveals Accelerated Conformational Changes in Iodoretinal-Substituted Proteorhodopsin. *Biophys. J.* **2011**, *101*, 1345−1353.
(60) Kim, J.; Lee, J. H.; Kim, J.; Jun, S.; Kim, K. H.; Kim, T. W.; Wulff, M.; Ihee, H. Structural Dynamics of 1,2-Diiodoethane in Cyclohexane Probed by Picosecond X-ray Liquidography. *J. Phys. Chem. A* **2012**, *116*, 2713−2722.
(61) Kim, K. H.; Muniyappan, S.; Oang, K. Y.; Kim, J. G.; Nozawa, S.; Sato, T.; Koshihara, S.; Henning, R.; Kosheleva, I.; Ki, H.; Kim, Y.; Kim, T. W.; Kim, J.; Adachi, S.; Ihee, H. Direct Observation of Cooperative Protein Structural Dynamics of Homodimeric Hemoglobin from 100 ps to 10 ms with Pump−Probe X-ray Solution Scattering. *J. Am. Chem. Soc.* **2012**, *134*, 7001−7008.
(62) Kim, T. W.; Lee, J. H.; Choi, J.; Kim, K. H.; van Wilderen, L. J.; Guerin, L.; Kim, Y.; Jung, Y. O.; Yang, C.; Kim, J.; Wulff, M.; van Thor, J. J.; Ihee, H. Protein Structural Dynamics of Photoactive Yellow Protein in Solution Revealed by Pump−Probe X-ray Solution Scattering. *J. Am. Chem. Soc.* **2012**, *134*, 3145−3153.
(63) Ihee, H.; Cao, J.; Zewail, A. H. Ultrafast electron diffraction: structures in dissociation dynamics of $Fe(CO)_5$. *Chem. Phys. Lett.* **1997**, *281*, 10−19.
(64) Ihee, H.; Cao, J.; Zewail, A. H. Ultrafast Electron Diffraction of Transient $[Fe(CO)_4]$: Determination of Molecular Structure and Reaction Pathway. *Angew. Chem., Intl. Ed. Engl.* **2001**, *40*, 1532−1536.
(65) Ihee, H.; Lobastov, V. A.; Gomez, U. M.; Goodson, B. M.; Srinivasan, R.; Ruan, C.; Zewail, A. H. Direct Imaging of Transient Molecular Structures with Ultrafast Diffraction. *Science* **2001**, *291*, 458−462.
(66) Ihee, H.; Feenstra, J. S.; Cao, J.; Zewail, A. H. Ultrafast Electron Diffraction of Transient Cyclopentadienyl Radical: A Dynamic Pseudorotary Structure. *Chem. Phys. Lett.* **2002**, *353*, 325−334.
(67) Ihee, H.; Goodson, B. M.; Srinivasan, R.; Lobastov, V. A.; Zewail, A. H. Ultrafast Electron Diffraction and Structural Dynamics: Transient Intermediates in the Elimination Reaction of $C_2F_4I_2$. *J. Phys. Chem. A* **2002**, *106*, 4087−4103.
(68) Hohenberg, P.; Kohn, W. Inhomogeneous Electron Gas. *Phys. Rev. B* **1964**, *136*, 864−871.
(69) Kohn, W.; Sham, L. J. Self-Consistent Equations Including Exchange and Correlation Effects. *Phys. Rev. A* **1965**, *140*, 1133−1138.
(70) Raghavachari, K.; Trucks, G. W.; Pople, J. A.; Headgordon, M. A 5th-Order Perturbation Comparison of Electron Correlation Theories. *Chem. Phys. Lett.* **1989**, *157*, 479−483.
(71) Perutz, R. N.; Turner, J. J. Photochemistry of the Group 6 hexacarbonyls in low-temperature matrixes. IV. Tetracarbonylmolybdenum and tricarbonylmolybdenum. *J. Am. Chem. Soc.* **1975**, *97*, 4800−4804.
(72) Roos, B. O. Advances in Chemical Physics. *Ab Initio Methods in Quantum Chemistry II*; John Wiley and Sons: Chichester, England, 1987.
(73) Andersson, K.; Malmqvist, P. A.; Roos, B. O. 2nd-Order Perturbation-Theory with a Complete Active Space Self-Consistent Field Reference Function. *J. Chem. Phys.* **1992**, *96*, 1218−1226.
(74) Andersson, K.; Malmqvist, P. A.; Roos, B. O.; Sadlej, A. J.; Wolinski, K. Second-Order Perturbation Theory with a CASSCF Reference Function. *J. Phys. Chem.* **1990**, *94*, 5483−5488.
(75) Finley, J.; Malmqvist, P. A.; Roos, B. O.; Serrano-Andres, L. The Multi-State CASPT2 Method. *Chem. Phys. Lett.* **1998**, *288*, 299−306.
(76) Roos, B. O.; Lindh, R.; Malmqvist, P. A.; Veryazov, V.; Widmark, P. O. Main Group Atoms and Dimers Studied with a New Relativistic ANO Basis Set. *J. Phys. Chem. A* **2004**, *108*, 2851−2858.
(77) Hess, B. A. Relativistic Electronic-Structure Calculations Employing a Two-Component No-Pair Formalism with External-Field Projection Operators. *Phys. Rev. A* **1986**, *33*, 3742−3748.
(78) Jansen, G.; Hess, B. A. Revision of the Douglas−Kroll Transformation. *Phys. Rev. A* **1989**, *39*, 6016−6017.
(79) Roos, B. O.; Lindh, R.; Malmqvist, P. A.; Veryazov, V.; Widmark, P. O. New Relativistic ANO Basis Sets for Transition Metal Atoms. *J. Phys. Chem. A* **2005**, *109*, 6575−6579.
(80) Lee, E. P. F.; Lozeille, J.; Soldan, P.; Wright, T. G. Calculations on the unstable CO^- ($X^2\Pi$) anion. *Chem. Phys. Lett.* **2001**, *336*, 479−487.
(81) Balabanov, N. B.; Peterson, K. A. Systematically Convergent Basis Sets for Transition Metals. I. All-Electron Correlation Consistent Basis Sets for the 3d Elements Sc−Zn. *J. Chem. Phys.* **2005**, *123*, 64107.
(82) Karlstrom, G.; Lindh, R.; Malmqvist, P. A.; Roos, B. O.; Ryde, U.; Veryazov, V.; Widmark, P. O.; Cossi, M.; Schimmelpfennig, B.; Neograd, P.; Seijo, L. MOLCAS: A Program Package for Computational Chemistry. *Comput. Mater. Sci.* **2003**, *28*, 222−239.
(83) Ehlers, A. W.; Frenking, G.; Baerends, E. J. Structure and Bonding of the Noble Gas−Metal Carbonyl Complexes $M(CO)_5$−Ng (M = Cr, Mo, W and Ng = Ar, Kr, Xe). *Organometallics* **1997**, *16*, 4896−4902.
(84) Zhou, M. F.; Andrews, L.; Bauschlicher, C. W. Spectroscopic and Theoretical Investigations of Vibrational Frequencies in Binary Unsaturated Transition-Metal Carbonyl Cations, Neutrals, and Anions. *Chem. Rev.* **2001**, *101*, 1931−1961.
(85) Harvey, J. N.; Aschi, M. Modelling Spin-Forbidden Reactions: Recombination of Carbon Monoxide with Iron Tetracarbonyl. *Faraday Discuss* **2003**, *124*, 129−143.
(86) Tsuchiya, T.; Roos, B. O. A Theoretical Study of the Spin-Forbidden Reaction $Fe(CO)_4$+CO→$Fe(CO)_5$. *Mol. Phys.* **2006**, *104*, 1123−1131.